ACS APPLIED NANO MATERIALS

www.acsanm.org Article

Enhanced Optical Absorption of GaAs Near-Band-Edge Transitions in GaAs/AlGaAs Core–Shell Nanowires: Implications for Nanowire Solar Cells

Arianna Cretì,[§] Paola Prete,[§] Nico Lovergine,* and Mauro Lomascolo

Cite This: *ACS Appl. Nano Mater.* 2022, 5, 18149–18158

Read Online

ACCESS | Metrics & More | Article Recommendations | Supporting Information

ABSTRACT: Dense arrays of core–shell nanowires possess great potential as superabsorptive media for the fabrication of efficient solar cells. We report on GaAs near-band-edge absorption properties of free-standing GaAs–AlGaAs core–shell nanowires having different shell thicknesses, by detailed line-shape analyses of room-temperature photoreflectance (PR) spectra, employing first-derivative Gaussian and Lorentzian models of the GaAs complex dielectric function. Line-shape analyses of the nanowire PR spectra returned a doublet of resonance lines at energies between 1.410 and 1.422 eV, ascribed to strain-split heavy- and light-hole exciton absorption transitions in the GaAs nanowire cores. The optical oscillator strengths of exciton resonances evaluated by Lorentzian analyses of PR features showed a significant enhancement (up to 30×) of GaAs band-edge optical absorption in nanowires with respect to the reference planar structure. Additionally, values of integrated Lorentzian moduli were normalized to the total GaAs core volume fill fraction (estimated in the range 0.5–7.0% with respect to a planar layer of the same height) within each nanowire ensemble, achieving a first ever experimental estimate of the GaAs near band-edge absorption enhancement factor for GaAs–AlGaAs core–shell nanowires in the range 22–190, depending on the nanowire inner core–shell structure. Such strong absorption enhancement is ascribed to improved wave-guiding of incident light into the GaAs cores by the surrounding AlGaAs shell (its average thickness being estimated between ∼14 and 100 nm in the present nanostructures).

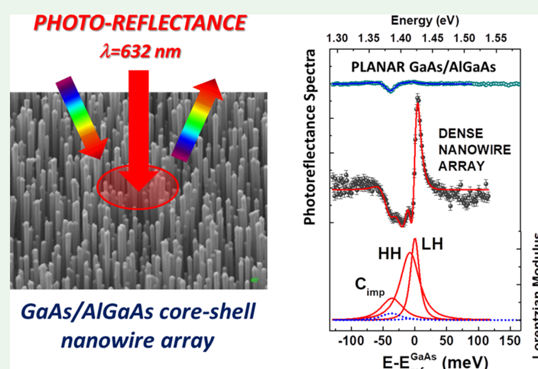

KEYWORDS: *III-V compounds, GaAs–AlGaAs core–shell nanowires, photoreflectance spectroscopy, near band-edge transitions, enhanced optical absorption, nanowire solar cells*

Downloaded via 93.40.194.193 on December 23, 2022 at 12:05:00 (UTC).
See https://pubs.acs.org/sharingguidelines for options on how to legitimately share published articles.

■ INTRODUCTION

Free-standing nanowires based on compound semiconductors continue to attract considerable research interests due to their applications to a variety of novel nanophotonic devices.[1−3] In particular, dense arrays of III-V-based core–shell nanowires have shown great potential for the fabrication of efficient solar cells: while unpassivated radial p–n junction GaAs nanowire solar cells were first reported in 2009 with a power conversion efficiency (PCE) of 0.83% under 1-sun irradiation,[4] passivation of such GaAs nanowires by InGaP shells was shown to increase the cell efficiency up to 6.63%.[5] A conversion efficiency of 15.3% under 1-sun illumination has been further reported in 2016 for axial p-n junction nanowire array solar cells,[6] in which GaAs nanowires were overgrown by an AlGaAs shell for passivation purposes. A record-high PCE of 17.8% has been instead, reported for InP-based solar cells.[7]

The use of nanowires offers significant physical and fabrication advantages over conventional (planar) photovoltaic devices due to their peculiar optical properties: indeed, (i) light-trapping effects associated with local and guided resonance modes in dense nanowire arrays allow high optical absorptance of solar radiation,[8−10] thus removing the need for antireflection coatings. For periodic arrays of GaAs nanowires with optimized geometry, a 500% increase in photon absorption per unit volume has been calculated, leading to estimation of a solar cell PCE of 22.3%.[9] In passivated core–shell nanowires, light wave-guiding is expected with a proper choice of the outer shell material bandgap and thickness, leading to a stronger increase of optical absorption with respect to unpassivated nanowires.[11] Furthermore, (ii) because of their reduced (subwavelength) lateral dimensions single-nanowire devices can absorb light from an area much larger than their own size, a nanoantenna effect relevant to photovoltaics: cross-sectional areas for photon absorption near the fundamental

Received: September 13, 2022
Accepted: November 10, 2022
Published: December 1, 2022

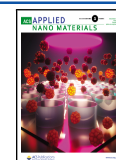

ACS Publications © 2022 The Authors. Published by American Chemical Society

bandgap around 1×10^6 nm^2 have been calculated by Krogstrup et al. (ref 12) for 380 nm-diameter single GaAs nanowires. As a result of light concentration, exceptionally high open-circuit photocurrents have been estimated by the above authors for single core−shell p−n junction GaAs nanowires, with estimated PCEs apparently beyond the Shockley−Queisser limit. It is worth noting that the large cross-sectional areas associated with the nanoantenna effect would lower the nanowire density necessary to efficiently absorb solar photons incident on a nanowire array down to the 10^8 cm^{-2} range; these densities correspond to overall nanowire volumes well below 10% (see present results) of that required for a planar epilayer, ensuring a strong reduction in the amount of costly III-V materials employed in the cell fabrication.

Despite the breath of different nanowire heterostructures proposed for solar cells,[13−15] to date direct experimental estimates of absorption enhancement remain mostly limited to single[16] or dense arrays[17] of compositionally uniform nanowires. In this paper, we study the optical properties of free-standing GaAs/$Al_{0.33}Ga_{0.67}As$ core−shell nanowire arrays of different densities by means of highly resolved room-temperature photoreflectance (PR) measurements. The high sensitivity and spectral resolution of PR spectroscopy in conjunction with appropriate line-shape analysis methods of experimental data allowed us to determine the nature of GaAs near band-edge resonances and estimate their oscillator strengths. Comparison with planar GaAs/AlGaAs/GaAs heterostructures evidenced strongly enhanced optical absorption for present nanowires; GaAs volume-normalized enhancement factors were then carefully estimated for the first time through detailed analysis of the nanowire dimensions and density within the arrays, conducted by means of high-resolution scanning electron microscopy. Our work investigated the potential of present core−shell nanowires as superabsorptive media in photovoltaic applications and evidenced the dependence of the enhanced GaAs absorption efficiency on the nanowire inner core−shell structure.

■ EXPERIMENTAL METHODS

Core−Shell Nanowire Growth. Dense arrays of free-standing GaAs−AlGaAs core−shell nanowires were grown on semi-insulating (111)B-GaAs wafers by metalorganic vapor phase epitaxy (MOVPE) (Scheme 1). [111]-oriented GaAs core nanowires were grown at 400 °C by the vapor−liquid−solid method, employing colloidal Au-nanoparticles (NPs) in aqueous solution with diameters in the 70−80 nm range as catalysts. The number of colloidal solution drops poured onto the substrate was locally varied, obtaining different NP densities (and correspondingly different densities of grown GaAs nanowires) across its surface. A relatively thick shell of $Al_xGa_{1-x}As$ (with $x = 0.33$, refs 18, 19) followed by a thin GaAs capping shell (the latter to avoid oxidation of the AlGaAs alloy when exposed to atmosphere) was then overgrown at 650 °C around the GaAs nanowires by conventional MOVPE under As-rich vapor conditions. The AlGaAs shell and GaAs cap layer growth times were, respectively, 10 and 1 min. Further details of the growth procedure and MOVPE parameters employed are reported in refs 20, 21. A portion of each substrate was intentionally left free of catalyst NPs to ensure the growth of a (111)-oriented GaAs/AlGaAs/GaAs planar heterostructure (nominal thickness values for each epilayer ~7/215/21 nm, respectively) as reference for our optical study. As this concerns the GaAs band-edge absorption of [111]-oriented nanowire cores, comparison with the case of material volumes grown at the same temperature with identical crystal orientation appears meaningful.

Scheme 1. Schematics of Process Steps for the Synthesis of GaAs−AlGaAs Core−Shell Nanowires

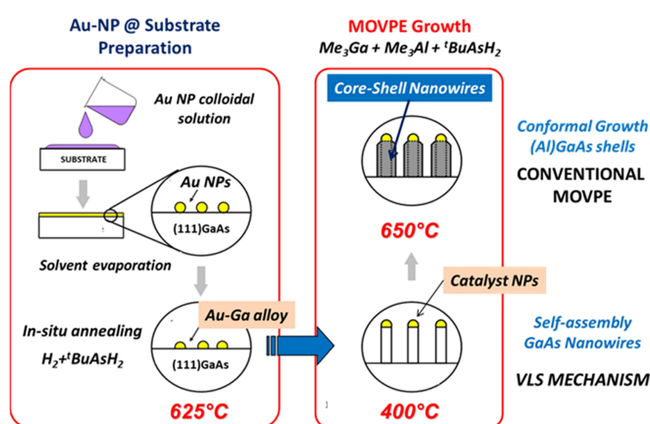

Morphological Analysis. The morphology and size of as-grown core−shell nanowires were studied by high-resolution field-emission scanning electron microscopy (FE-SEM) using a Zeiss Sigma VP microscope, equipped with a Gemini electron column and a 5 keV primary electron beam. A quantitative study of the nanowire geometric parameters (e.g., their lengths, diameters, and densities) was performed by FE-SEM observations of nanowire ensembles at particular areas across the sample surface, where PR measurements were afterward performed. The areas were selected by a combination of optical microscopy (Rayleigh scattering) and FE-SEM inspection so to have relatively homogeneous (over a few tenths of mm^2) nanowire densities, ensuring a consistent and meaningful spatial correlation between FE-SEM analysis and PR measurements. Further insights into the inner structural properties of present nanowires are reported in refs 22, 23.

PR Experiments. PR measurements were performed at room temperature on GaAs/AlGaAs core−shell nanowire ensembles still on their original growth substrate and the planar GaAs/AlGaAs/GaAs heterostructure (in the following, the reference sample) using a monochromatized 150 W halogen-tungsten lamp source and a 1 mW He-Ne laser (632.8 nm, 1.959 eV line) beam mechanically chopped at 233 Hz as an external periodic modulation signal. The He-Ne line is almost resonant to the $Al_{0.33}Ga_{0.67}As$ alloy nominal bandgap (1.905 eV at RT)[24] and ensures that the modulation beam is not completely absorbed by the relatively thin AlGaAs shells (for nanowires) or planar epilayer (for the reference heterostructure).[25]

The measurements were performed in backscattering geometry, resulting in the nanowires being illuminated from the top. Particular care was devoted to the signal collecting geometry and sample excitation, due to the reduced specular reflected signal, which originates from (i) the high optical absorption of nanowires; (ii) the light-trapping effect due to multiple light scattering within the nanowire array, and consequently (iii) a large diffused component. The spectral resolution achieved in these experiments has been varied in the 3−31 meV range (depending on the reflected intensity of the samples). The relative change in reflectance is reported as the $\Delta R(\lambda)/R(\lambda)$ signal, where $\Delta R(\lambda)$ and $R(\lambda)$ are the AC-modulated and DC average reflectance signals, respectively.

During the measurements, both the in-phase and out-of-phase components of the signal have been acquired. In phase-sensitive techniques, such as PR spectroscopy, it is possible to acquire simultaneously the in-phase and out-of-phase (or quadrature, i.e., shifted by 90° with respect the in-phase signal) components, which are related to processes with different time response to the external modulation field inducing the change in dielectric function.[26−28] In particular, a slower signal is expected to be more evident in the out-of-phase component.[26] Therefore, comparison between the results of line-shape analysis of the two (in-phase and out-of-phase) components allows us to discern the nature of different interactions occurring within the nanostructures due to both external modulation and optical excitation. In all the reported experiments, we adjusted the

https://doi.org/10.1021/acsanm.2c04044
ACS Appl. Nano Mater. 2022, 5, 18149−18158

phase in order to maximize the signal of the investigated resonance in the in-phase channel.

THEORETICAL BASIS

Line-Shape Analysis of PR Spectra. It is well known that because of its differential nature, optical modulated spectroscopy needs line-shape analysis of measured spectra in order to access experimental observables, such as the energy, phenomenological broadening, and oscillator strength of detected optical resonances. Several review papers have been reporting on these issues in the last decade.[29−31]

It has been shown that for optical transitions at room temperature the more appropriate profile for the complex dielectric function ε is Gaussian-like:[29,31−35]

$$\varepsilon(z, \Gamma, I) = \varepsilon_1 + i\varepsilon_2 = 1 + z\frac{I}{\Gamma}\Phi\left(1, \frac{3}{2}; -\frac{z^2}{2}\right) + i\sqrt{\frac{\pi}{2}}\frac{I}{\Gamma}\exp\left(-\frac{z^2}{2}\right); \quad z = \frac{E_{ph} - E}{\Gamma}$$

where E_{ph} is the photon energy, E, Γ, and I are respectively, the energy, broadening, and intensity of each resonance, while Φ is the degenerate hypergeometric function.[36]

Moreover, it is generally accepted in the literature that the change induced in the dielectric function and consequently the shape of the PR line (at room temperature) has a first-derivative character, especially in the case of a confined system.[33−35]

However, in the case of two-dimensional electron transitions, a third-derivative Lorentzian line-shape analysis[37] with exponential $m = 3$ is a good approximation of the first-derivative Gaussian one:[29]

$$\frac{\Delta R}{R} = Re[Ae^{i\theta}(E - E_0 + i\Gamma)^{-m}]$$

where A and θ are the amplitude and phase parameters of the resonance, respectively. This approximation allowed us to evaluate analytically the oscillator strength of optical transitions; based on the Kramers−Kronig relations connecting the real and imaginary parts of the response function, it is in fact possible to define an analytical form of the PR modulus $|\Delta\rho(E)|$, the so-called Lorentzian modulus, given by:

$$|\Delta\rho| = \frac{|A|}{[(E - E_0)^2 + \Gamma^2]^{m/2}}$$

whose integrated area is directly related to the oscillator strength of the optical absorption transition.[29,30,38] Additionally, the Lorentzian modulus provides a better visualization of the optical resonances, as compared with the differential-like PR spectra.

The two line-shape analysis above return in most cases almost indistinguishable fit curves, and the same energy and broadening (Γ) values (taking into account that $\Gamma_L = 2\sqrt{2\ln 2}\,\Gamma_G \sim 2.35\Gamma_G$), within the standard best-fitting errors.

In this work, two different Gaussian first-derivative line-shape models have been used to reproduce the experimental PR spectra. In fact, depending on the low-dimensional system and on the dominant modulation mechanism, two different Gaussian line-shapes have been extendedly used in the literature. In the first one, referred in the following as the refractive Gaussian (RG) model, the reflectivity close to the band-edge is assumed to be dominated by a refractive mechanism, neglecting the absorption contribution.[32−34] In this case, the line-shape of PR spectra is governed by the modulation of the energy (E_i), broadening (Γ_i), and oscillator strength (I_i) of the corresponding resonance and, from a mathematical point of view, the model consists of a linear combination of the first-derivative components of the real part of the dielectric function with respect to E, Γ, and I:

$$\frac{\Delta R}{R} \propto a_E\frac{\partial\varepsilon_1}{\partial E} + a_\Gamma\frac{\partial\varepsilon_1}{\partial\Gamma} + a_I\frac{\partial\varepsilon_1}{\partial I}$$

In the second model, referred to as the refractive and absorptive Gaussian (RAG) model, both the absorption and refractive mechanisms are considered. The RAG model takes into account both the real and imaginary parts of the dielectric function, assuming the optical response modulation as essentially due to the resonance energy modulation E_i, neglecting its broadening and oscillator strength.[29,30,35] In this case, from a mathematical point of view, the model consists of a linear combination of the first-derivative components with respect to E_i of both the real and imaginary parts of the dielectric function:

$$\frac{\Delta R}{R} \propto a_E\frac{\partial\varepsilon_1}{\partial E} + b_E\frac{\partial\varepsilon_2}{\partial E}$$

RESULTS AND DISCUSSION

Figure 1 shows the morphology of free-standing GaAs−AlGaAs core−shell nanowires across selected areas of the same sample. The nanowires grew with the ZB crystal phase and a low density of stacking faults in their trunk (see the Supporting Information) in the form of straight (kink-free) segments, with hexagonal cross-sections and bound by six sidewall ⟨110⟩ facets − see Figure 1b, their diameter being almost constant over their entire length.[21] Their density varies across the sample as a result of the inhomogeneous distribution of Au NPs on the substrate surface prior to growth (see Experimental Methods); as-grown nanowires are vertically well-aligned (yield >99%)[39] in most cases (Figure 1a,c,d), but for very high (>10^9 cm^{-2}) NP densities (Figure 1e). It is noteworthy that long and thin nanowire arrays may sometimes appear bent and attached to each other's by their tips (see Figure 1d), a

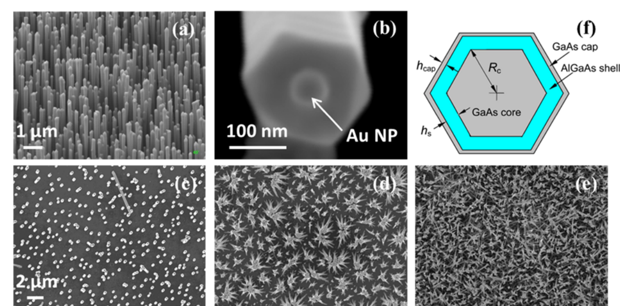

Figure 1. FE-SEM micrographs of (a) (45°-tilted view) GaAs−AlGaAs core−shell nanowires vertically aligned on their GaAs substrate, and (b) (magnified plan-view) of one particular nanowire from (a); (c−e) FE-SEM micrographs (plan-view, 10,000× magnification) of core−shell nanowires recorded at different positions (namely Areas A, B, and C) across the sample; (f) cross-sectional schematic of the core−shell nanowire inner structure. The marker in (c) holds also for (d,e).

https://doi.org/10.1021/acsanm.2c04044
ACS Appl. Nano Mater. 2022, 5, 18149−18158

Table 1. Average Au NP Diameter (D_{Au}), Overall Diameter (D), and Length (L) of GaAs−AlGaAs Core−Shell Nanowires and Their Local Substrate Density (δ), as Measured/Estimated from Analyses of FE-SEM Micrographs Recorded at Different Selected Areas (Namely, A, B, and C in Figure 1) of the Same Sample[a]

	FE-SEM measurements				shell growth model		
sample area	D_{Au} (nm)	D (nm)	L (μm)	δ (cm^{-2})	$L\delta$ (nm^{-1})	h_s (nm)	h_{cap} (nm)
A	74.6 ± 1.9	276.9 ± 2.2	6.4 ± 0.1	8.20×10^7	5.45×10^{-3}	99.9	1.2
B	70.2 ± 1.8	159.2 ± 1.6	7.1 ± 0.1	3.99×10^8	2.30×10^{-2}	41.7	0.5
C	80.0 ± 2.4	<99.5[b]	7−14	>1×10^9	n.d.	<14.2[b]	<0.3[b]

[a]The corresponding AlGaAs (h_s) and GaAs (h_{cap}) shell average thicknesses were calculated based on the growth model reported in ref 41, and assuming a GaAs core diameter proportional to D_{Au}. Values of $L\delta$ in the table are the model free-parameter best-fitting the experimental data. [b]Expected values based on the shell growth model.

result of dielectrophoretic forces induced by the primary electron beam during FE-SEM observations.[40] The residual catalyst NP diameter at the nanowire tips (D_{Au}), the nanowire overall diameter (D), and length (L)—see the nanowire schematic in Figure 1f—were estimated from statistical analysis of FE-SEM micrographs (see the Supporting Information) and correlated with the local (on the substrate) nanowire density (δ). The nanowire diameter D appears to decrease with increasing their density δ (Table 1), an effect driven by the vapor mass-transport controlled overgrowth of (Al)GaAs shells around dense GaAs nanowire arrays.[41] A quantitative model of the effect of precursors vapor mass transport on the nanowire shell growth rates predicts a nonlinear dependence on the actual (i.e., across the sample) value of $L\delta$, initial GaAs nanowire diameters (taken proportional to the Au catalyst NP size D_{Au}), and deposition times: details of the experimental validation of the shell growth model were provided in refs 41, 42. Here, the growth model is employed to best-fit the FE-SEM measured core−shell nanowire average diameters reported in Table 1 to predict the actual thickness of their AlGaAs and GaAs shells in each of the sample areas selected for PR measurements (see below), using the quantity $L\delta$ as a free-parameter and the average GaAs core diameters and shell growth times as input figures; best-fitting $L\delta$ values for Areas A and B in Table 1 are within a few percent of experimental values.

Figure 2 reports the in-phase PR spectra recorded with intermediate spectral resolution (7 meV) from a GaAs−AlGaAs core−shell nanowire ensemble (corresponding to Area A in Figure 1c) and the reference sample. The out-of-phase PR spectrum for Area A is also reported in the same figure. The PR spectrum of the reference sample presents an asymmetric resonance feature close to the GaAs bandgap. Lorentzian and Gaussian models return almost indistinguishable fit curves, with energies of the component resonances of 1.39 eV (Γ_L = 40 meV) and 1.425 eV (Γ_L = 55 meV). The feature at 1.39 eV can be assigned to carbon acceptor impurities in GaAs (bound-to-free transitions) as reported in the literature for PR experiments performed on similar GaAs/AlGaAs planar layers.[43−46] The resonance related to the GaAs bandgap (1.425 eV at RT) is instead quite broadened if compared with values typically observed in epitaxial structures.[43] A quite weaker and noisy resonance is also observed at around 1.78 eV, most probably related to the spin-orbit split-off band (Δ_{SO}) expected at 1.77 eV (i.e., 0.341 eV above the GaAs energy bandgap).[47,48]

The in-phase PR spectrum of the GaAs/AlGaAs core−shell nanowire ensemble reported in Figure 2 presents instead a very sharp and intense (about 5× stronger than for the reference sample) resonance feature at 1.42 eV, which appears broadened on its low-energy side. Both Lorentzian and Gaussian line-shape analyses of the nanowire spectrum return two resonances at 1.39 eV (Γ_L = 44 meV) and 1.425 eV (Γ_L = 21 meV). An additional symmetric single resonance is clearly visible at about 1.78 eV (Lorentzian line-shape analysis, continuous red line through the data), again consistent with the Δ_{SO} band of GaAs, as previously discussed for the reference sample.

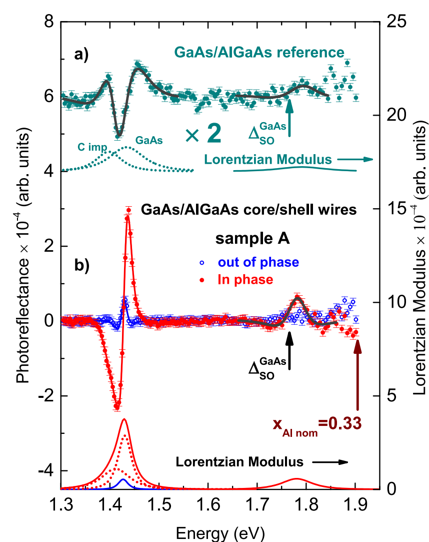

Figure 2. In-phase PR spectrum of (a) reference sample and (b) GaAs−AlGaAs core−shell nanowire ensemble (Area A in Figure 1) (green and red solid points, respectively), recorded at 7 meV spectral resolution. The continuous curves through experimental points represent the Lorentzian line-shape best-fitting of the spectra. The out-of-phase PR spectrum for the nanowire ensemble is also reported (open blue points). Comparison between the calculated Lorentzian moduli of the PR resonances is also shown for the three spectra. Dotted lines refer to each Lorentzian modulus components. The PR spectrum and Lorentzian moduli relative to the reference sample have been multiplied by a factor of two for the sake of clarity.

Particular care must be taken in the analysis and attributions of above resonances, in particular whether they originate from the nanowires or the underlying (i.e., grown on the catalyst-free surface between the nanowires) GaAs/AlGaAs/GaAs planar heterostructure. Indeed, in the case of dense nanowire arrays, both the probe beam and the modulating light would be almost totally absorbed from the nanowires, thus preventing the possibility to detect a signal coming from the underlying planar heterostructure. This is especially true for PR spectra recorded from Areas B and C of the sample (Figure 1d,e), as further discussed in the following. In the case of the PR spectrum in Figure 2, the measured nanowire density (~8 ×

https://doi.org/10.1021/acsanm.2c04044
ACS Appl. Nano Mater. 2022, 5, 18149−18158

10^7 cm^{-2}) corresponds to a nanowire-to-nanowire average distance of ∼1.4 μm (see Figure 1), that is, well above the wavelength corresponding to the GaAs band-edge (λ_{GaAs} = 865 nm at RT); therefore, a contribution due to the planar heterostructure in between the nanowires could not be completely ruled out based on the sole in-phase PR signal.

The observation of a non-negligible out-of-phase component in the PR spectrum corresponding to Area A (blue open circles in Figure 2) indicates the occurrence of an additional response process with a longer time-scale (probably due to thermal effects), originating either in the nanowire GaAs cores or from the underlying planar GaAs/AlGaAs/GaAs heterostructure, which weakly contribute to the reflectivity with a different phase/time-constant with respect to the external modulation. This component presents a quite different spectrum, if compared with the in-phase one, presenting a weak and sharp resonance at 1.415 meV (Γ_L = 15 meV, single Lorentzian line-shape analysis). The out-of-phase PR spectrum is consistent, both in shape and amplitude, with the in-phase one measured on the reference sample. Furthermore, a much weaker and scattered signal is also present at about 1.78 eV. These results strongly suggest that the out-of-phase component of the nanowires arises from the underlying planar heterostructure; it confirms in turn that the in-phase PR spectrum recorded from the sample Area A predominantly originates from the core−shell nanowires.

As already mentioned, besides providing a clear visualization of the resonances, the integrated area of each resonance Lorentzian modulus is directly related to the oscillator strength of the optical transition. For all the above identified resonances, their Lorentzian modulus has been thus reported in Figure 2; from the diagrams, a significant enhancement of optical absorption in the core-shell nanowires compared to the planar reference sample can be deduced. The implication of this finding will be discussed more in-depth later on.

To explain the nature of the asymmetric resonance in the in-phase PR spectrum of GaAs nanowires, we performed PR experiments by increasing the spectral resolution up to 3 meV, which is the highest resolution achievable compatibly with the weak reflected signal intensity of present samples. The result is reported in Figure 3; the broadened shoulder at low energy observed in Figure 2 manifests now a rich structure with at least three clear oscillations occurring within 70 meV below the GaAs band edge. Therefore, such oscillations cannot be ascribed to Franz−Keldysh oscillations.[29−31] We also notice that the weaker resonance observed in the high-resolution PR spectrum of the reference sample (also reported in Figure 3) is not as structured as the one recorded from the nanowires. Additionally, these oscillations only arise from the modulated component of PR spectra and are not present in the continuous reflectivity signal. However, to estimate any interference effects originating from the underlying planar heterostructure, a line-shape analysis including multilayer interference effects[35,49−51] has been also performed. The simulation of PR spectra (not shown here) taking into account the parameter of the GaAs/AlGaAs/GaAs reference sample (layer thickness, refractive indexes, extinction coefficients, etc.) does not reproduce the experimental PR spectra reported in Figure 3. This confirms that the structured resonance is related to transitions within the GaAs cores. To further clarify the origin of the structured resonance in the nanowire PR spectrum of Figure 3 and identify the associated energy transitions, we performed both Lorentzian and Gaussian

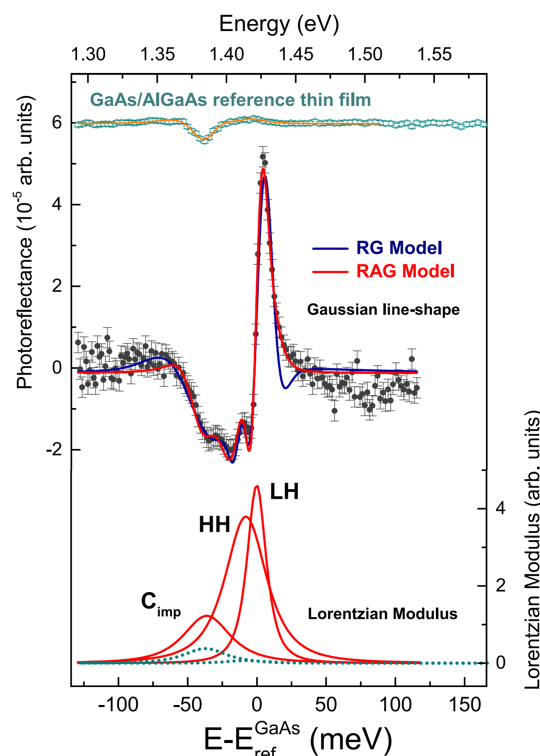

Figure 3. PR spectra (recorded under 3 meV spectral resolution) from the GaAs−AlGaAs core−shell nanowire ensemble (same area as in Figure 2) and the reference sample. The continuous lines through the nanowire spectrum are the Gaussian line-shape best-fit of experimental data performed with the RAG and RG models (red and blue lines, respectively). For each model, three resonances have been used (see Table 1). The calculated Lorentzian modulus for each resonance is also reported in the lower part of the diagram.

analyses. In particular, three resonances (e_1, e_2, and e_3 in the following) have been used in the analyses by the RG and RAG models: the results of the spectrum line-shape best-fittings by these models are reported in Figure 3 in the form of continuous (red and blue, respectively) lines through experimental data; best-fitting energy resonances E_i and broadening parameters Γ_i corresponding to the e_1, e_2, and e_3 resonances are reported in Table 2. In particular, the RAG analysis returned three well-resolved resonances, the one at 1.421 eV being quite narrow, its Gaussian line broadening being Γ_G = 5 meV (about one-half that of the other two resonances). For comparison, a two-resonance RGA line-shape analysis was performed on the high-resolution PR spectrum of the AlGaAs/GaAs reference structure, and the result is also reported in Figure 3.

The following general remarks can be highlighted from the results of our analysis by the RG and RGA models: (i) both models provide the same energy values, within best-fit uncertainties, for all resonances with the only exception of e_1 (which appears slightly red-shifted in the RG estimate); (ii) even though the RG model includes four more fitting-parameters for each resonance, it essentially fails in describing the high-energy tail of the PR spectrum, that is, in the GaAs absorption range; (iii) the RAG model gives instead an excellent fit across the full spectral range, confirming that the PR modulation mechanism in the nanowires is mainly related to the induced variation of energy levels and that the

https://doi.org/10.1021/acsanm.2c04044
ACS Appl. Nano Mater. 2022, 5, 18149−18158

Table 2. Energy Resonances E_i and Corresponding Broadening Γ_i Resulting from the Line-Shape Analysis by Means of the RG and RAG Models Employing Three Resonances (e_1, e_2, e_3)[a]

	model RG: $\Delta R/R \sim a\Delta\varepsilon_1$ chi-sqr 0.66; adj R-square 0.88		model RAG: $\Delta R/R \sim a\Delta\varepsilon_1 + b\Delta\varepsilon_2$ chi-sqr 2.9; adj R-square 0.91326	
	E_i (eV)	Γ_i (eV)	E_i (eV)	Γ_i (eV)
e_1	1.381 ± 0.001	0.017 ± 0.001	1.386 ± 0.008	0.009 ± 0.002
e_2	1.4095 ± 0.0007	0.005 ± 0.004	1.413 ± 0.003	0.011 ± 0.002
e_3	1.4225 ± 0.0003	0.0075 ± 0.0002	1.421 ± 0.001	0.0046 ± 0.0003

[a]The error refers to standard deviations as returned by the χ^2 minimization procedure.

absorptive imaginary counterpart of the dielectric function cannot be neglected (as in the RG model).

It is noteworthy that the Lorentzian analysis of the nanowire PR spectrum in Figure 3 returned a line-shape fitting and energies of the resonances undistinguishable from that of Gaussian ones but allowed determining the optical oscillator strengths of the resonances, further elucidating the nature of e_1, e_2, and e_3 transitions. As-obtained Lorentzian moduli are reported in Figure 3, together with those of the reference sample.

The resonances in Table 2 have been consequently assigned as follows: present GaAs nanowires were previously shown to be slightly p-type,[52] most likely as a result of unintentional carbon incorporation during MOVPE growth. Resonance e_1 (at 1.386 eV) has been thus ascribed to a bound-to-free transition involving carbon acceptor impurities within the GaAs cores. It is noteworthy that this resonance appears to have a larger intensity and a comparable Lorentzian linewidth (modulus-area ~6 × 10^{-6} and Γ_L = (26 ± 3) meV) for the nanowires with respect to what was observed in the reference sample (modulus-area ~2 × 10^{-6} and Γ_L = (21 ± 3) meV), despite the fact that the 21 nm thick GaAs epilayer within the planar structure (see the Experimental Section) is expected to be fairly carbon-doped because of its low growth temperature.

Resonance e_3 (at 1.421 eV) appears very narrow with a broadening parameter Γ_{G3} = 4.6 meV (i.e., comparable to values observed in the PR spectra of high quality AlGaAs/GaAs planar heterostructure[33,43]), while resonance e_2 (at 1.413 eV) appears red-shifted by ~8 meV with respect to e_3 and about 3× broader (Γ_{G2} = 11 meV). The significant difference in the phenomenological broadening parameters strongly suggests that e_2 and e_3 resonances could be ascribed to heavy (HH) and light-hole (LH)-related transitions, respectively. Indeed, it is well known that the natural line broadening of transitions involving HH and LH states is directly proportional (through the uncertainty principle) to their corresponding transition rates (R). The ratio between experimental values (Γ_{G2}/Γ_{G3}) = 2.4 is in good agreement with the value commonly reported in the literature[53,54] for the HH- to LH-related transition-rates ratio (R_{HH}/R_{LH}) = 3. In this respect, we highlight that the contribution of inhomogeneous broadening (related to disorder within the nanowires) scarcely affects the Γ_{G2}/Γ_{G3} ratio (see the Supporting Information) and our conclusion. The observation of exciton resonances in optical absorption spectra has been reported at room temperature for pure n- and p-type GaAs crystals[55] indeed supporting our previous claim that present GaAs cores are only lightly p-doped. Furthermore, the energy separation between e_2 and e_3 resonances is consistent with a tensile-strain-induced splitting of the GaAs HH-LH valence bands at the Γ point (see the Supporting Information).[56,57]

To better understand the role of absorption, as highlighted by the RAG model analysis, in the PR modulation mechanisms of present nanowire samples, we performed PR experiments on nanowire ensembles having higher densities (Areas B and C in Table 1). Because of the weak reflected signal associated with high-density nanowires and in order to increase the incident probe intensity, all measurements were performed at the lowest spectral resolution (31 meV). The results are reported in Figure 4a (upper section) together with the PR spectra

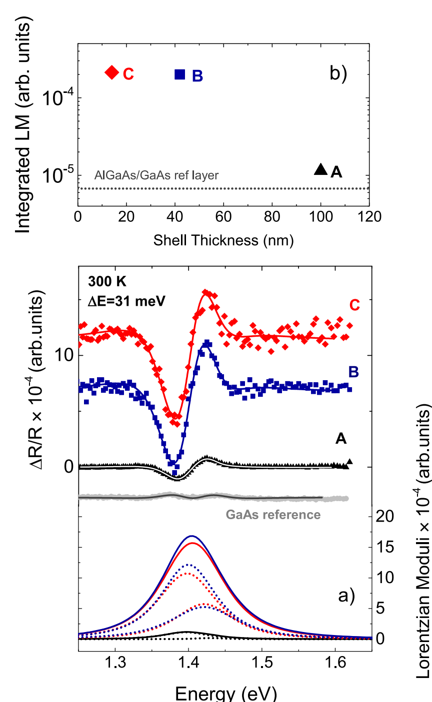

Figure 4. (a) Upper section: PR spectra of GaAs−AlGaAs core−shell nanowires arrays with different densities (Areas A, B, and C in Table 1). The continuous lines through experimental data are the Lorentzian line-shape best-fitting of PR spectra. Lower section: calculated Lorentzian moduli (LM) of PR resonances. (b) Values of the integrated LM as a function of estimated AlGaAs shell thickness h_s (see Table 1 for the latter).

recorded under the same conditions for medium density nanowires (Area A in Table 1) and the reference planar sample (squared gray symbols).

For the spectra in Figure 4, no clear evidence of PR resonance has been achieved in the Δ_{so} spectral range, while the out-of-phase components of the PR signals are negligible. On the contrary, all nanowire samples showed an intense resonance in the spectral range of GaAs band-edge, the resonance being asymmetric on its low-energy side. As previously discussed for the PR spectrum recorded on the sample Area A, such resonances can be ascribed to transitions occurring in the GaAs core nanowires. Most noticeably, we observe that the resonance signal in the PR spectra of Figure 4

https://doi.org/10.1021/acsanm.2c04044
ACS Appl. Nano Mater. 2022, 5, 18149−18158

increases as the nanowire density increases. However, measurements performed on Area A (lower nanowire density, larger shell) show the lowest $\Delta R(\lambda)/R(\lambda)$ signal, while the modulated $\Delta R(\lambda)$ and continuous $R(\lambda)$ signals are about 3× and 30× larger respectively, than those for the denser nanowire samples. Geometrical effects such as reduced light trapping induced by the lower nanowire density of Area A could explain the higher continuous signal $R(\lambda)$ observed for this sample. On the contrary, the high modulated signal $\Delta R(\lambda)$ suggests an enhanced optical modulation of the processes occurring in this sample.

A Lorentzian analysis has been applied to the PR spectra of the different nanowire ensembles; the resulting Lorentzian moduli of the PR resonances are also reported in Figure 4a. The analysis returned two energy resonances at 1.39 and 1.42 eV for all nanowire samples. However, the low spectral resolution of PR spectra does not allow any quantitative estimate in terms of resonance energy shift and/or broadening effects for the different nanowire samples. Anyway, a comparison between the Lorentzian moduli confirms an enhancement of the optical absorption of nanowire ensembles with increasing their density. This result is further highlighted in Figure 4b, where the integrated areas of the Lorentzian moduli are reported for each sample; noteworthy, PR spectra measured for Areas B and C, having the largest wire densities (Table 1), show integrated Lorentzian moduli about 30× larger than the reference sample.

A more valuable estimate of the absorption enhancement for present core−shell nanowires can be obtained by normalizing the integrated Lorentzian moduli to the actual GaAs core volume fill fraction (relative to a planar layer of the same thickness) of the nanowire ensembles. Based on data in Table 1, we calculated the GaAs volume fill fraction within the nanowire arrays to be 0.55−0.57% and 1.6−2.0% for Areas A and B, respectively (see the Supporting Information). Such values correspond to an equivalent GaAs film thickness l_{NW} of about 35−37 nm and 116−144 nm, respectively. For the sample Area C, we estimated instead, a volume fill fraction ~6.9% or higher, corresponding to l_{NW} roughly in the range 483−965 nm.

We therefore estimate the volume- and light-intensity-normalized exciton oscillator strengths for the reference sample and the nanowire arrays, as follows: taking F_{planar} as the Lorentzian modulus of exciton absorption estimated from our analyses of PR spectra of the reference sample (Figure 4), $(1 - R_{planar})I_0 \approx 0.7I_0$ as the incident light intensity effectively transmitted through the 215 nm thick AlGaAs layer reaching the underlying planar GaAs, and taking a near band-edge (i.e., at photon energies ~1.4 eV) absorption length $l_\alpha = 1 \times 10^3$ nm for the undoped GaAs substrate,[55] the normalized reference sample oscillator strength can be roughly calculated as $F_{planar}/(1 - R)I_0 l_\alpha$; similarly, if F_{NW} is the corresponding Lorentzian modulus for exciton absorption from nanowires, and considering that the optical reflection R_{NW} of their arrays is quite small, the normalized exciton oscillator strength for the nanowires can be simply estimated as $F_{NW}/I_0 l_{NW}$. The nanowire near band-edge absorption enhancement factor (with respect to the reference sample) can then be estimated by

$$(1 - R)\frac{F_{NW}}{F_{planar}}\left(\frac{l_\alpha}{l_{NW}}\right) \quad (1)$$

Application of eq 1 to sample Areas A and B leads to absorption enhancement factors of 32−34 and 153−190, respectively, where the value intervals arise from uncertainties in evaluating the GaAs core volume fill factors (see the Supporting Information). The estimated value for Area C turns out instead in the range of 22−43 or just below.

Such large absorption enhancement ratios indicate that incident light gets strongly absorbed in present nanowires. Krogstrup et al.[12] reported on the band-edge absorption of a 2.5 μm long free-standing GaAs nanowire embedded in SU-8 and a theoretically calculated enhancement factor of 10−70 (depending on its actual diameter) with respect to an equivalent thin film. It is noteworthy that our estimated enhancement factors appear comparable (for sample Areas A and C) or appreciably greater (for sample Area B) than those calculated in ref 12; however, multiple light scattering between nanowires must be also considered in determining the optical properties of dense nanowire arrays. For this purpose, a finite difference time-domain (FDTD) analysis is usually carried out.[8]

In Figure 5, the as-obtained enhancement factors for our core−shell nanowires are compared with volume-normalized

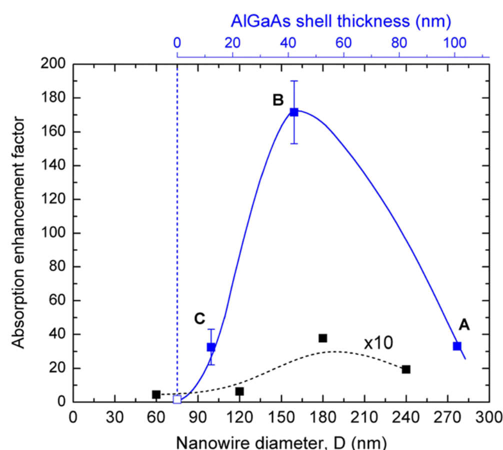

Figure 5. Estimated absorption enhancement factors as function of nanowire diameter in the case of GaAs−AlGaAs core−shell nanowire (blue solid points) and GaAs nanowire (black solid points) arrays. Values for GaAs arrays were calculated based on FDTD reflectance data reported in ref 9, while the light blue point represents the extrapolated value for 75 nm-diameter GaAs nanowires. The upper blue scale shows the average AlGaAs shell thickness (Table 1) of the core−shell nanowire ensembles corresponding to sample Areas A, B, and C. Black and blue lines are only guides for the eye.

values for dense periodic arrays of GaAs nanowires (having a fixed diameter-to-pitch ratio of 0.5, which corresponds to a volume fill fraction of 19.6%), estimated at λ = 876 nm on the basis of FDTD-simulated reflectance data reported in ref 9. It is noteworthy that the volume-normalized enhancement factors for the GaAs nanowire arrays remain always within the 0.4−3.8 range; in particular, values <1 (absorptance lower than for a thin film) are obtained for nanowire diameters <120 nm, as only a few resonance guided-modes are allowed within the nanowires;[11] as the nanowire diameter increases more guided-modes come into play, the enhancement factor increases. However, further increasing the diameter leads to a decrease in absorption efficiency due to increased reflection at the top surface of the nanowire array and insufficient field concentration at long wavelengths.[9] We further underline here

https://doi.org/10.1021/acsanm.2c04044
ACS Appl. Nano Mater. 2022, 5, 18149−18158

that taking volume fill fractions comparable to those found for our core−shell arrays (around 0.6−7%) would bring the calculated absorption enhancement factors of the GaAs nanowire arrays to values well below those shown in Figure 5.

In comparison, our core−shell nanowires show much higher (up to about 50× that of GaAs nanowires) absorption factors, despite the small average diameter (70−80 nm, Table 1) of their GaAs cores. Bao and Ruan[10] previously showed that while nanowire arrays with random position of individual nanostructures show small absorption enhancement with respect to uniform (periodic) arrays, those with random nanowire diameters or lengths may show significant absorption enhancement. However, our nanowire arrays present much narrower diameter and length distributions (see Table 1 and Supporting Information) than those reported in ref 10 for significant contribution to the absorption enhancement.

Our findings can be therefore ascribed to improved light wave-guiding into the GaAs cores induced by addition of the surrounding AlGaAs shell.[11] Still, our data mimic the nanowire diameter dependence observed for simple GaAs nanowires: for a very thin shell thickness the absorption enhancement remains relatively small, as in this case the guided-modes tend to be squeezed out of the GaAs core and onto the core−shell nanowire surface (air modes);[1,11] instead, increasing the shell thickness localizes the light more and more into the nanowires (dielectric resonance modes) allowing for higher absorption efficiencies. Finally, Figure 5 shows that, as for the GaAs nanowire arrays, large diameters of the core−shell nanowires (corresponding to lower nanowire densities) lead to a decrease of the absorption enhancement factor, as a result of increased optical reflectance from the array.

Detailed numerical comparison of our experimental absorption enhancement factors with those obtained by FDTD simulations remains however necessary for present core−shell nanowire arrays to confirm our conclusion and explore whether even larger values could be obtained by fine tuning of the nanowire geometrical parameters.

We would finally point out that, as the difference between the core and shell refractive indices remains almost constant within the investigated spectral range (600−820 nm),[58] our conclusions can be extended also to the case of PR measurements performed in GaAs-resonant modulation condition.

CONCLUSIONS

We reported on the optical study of GaAs near-band-edge absorption in free-standing GaAs−AlGaAs core−shell nanowires conducted through line-shape analyses of room-temperature PR spectra, the latter measured for nanowire arrays of different densities and, for the sake of comparison, planar GaAs/AlGaAs/GaAs epilayers. In all cases, PR resonances within the energy region of GaAs bandgap were clearly observed, allowing to perform meaningful fittings of PR spectra by employing first-derivative Gaussian models (i.e., Refractive and Refractive-Absorptive) of the GaAs complex dielectric function.

Under the highest PR spectral resolution (3 meV) compatible with the weak reflected signal intensity of the nanowire arrays, line-shape analyses through the above Gaussian models both returned a doublet of resonance lines at energies between 1.410 and 1.422 eV, and further ascribed to strain-split HH- and LH-exciton transitions within the GaAs core. The observation of exciton resonances in room-temperature PR spectra strongly indicate that the present GaAs core material is relatively pure. Still, a weaker resonance at 1.386 eV has been ascribed to a bound-to-free transition involving residual carbon acceptor impurities within the material.

The Lorentzian analyses of PR spectra returned line-shape fittings and resonance energies undistinguishable from that obtained from Gaussian ones; however, the former allowed determining the optical oscillator strengths of the exciton resonances, taken proportional to their Lorentzian modulus, the latter obtained by best-fitting PR spectra measured at various positions across the sample and corresponding to core−shell nanowire arrays of different densities. Significant enhancements (up to 30×) of the exciton optical absorption with respect to the reference GaAs/AlGaAs/GaAs planar structure were so demonstrated. A more valuable estimate of the absorption enhancement for present nanowires was then obtained by normalizing the integrated Lorentzian moduli to the estimated GaAs core volume fill fraction within each nanowire ensemble. Volume-normalized absorption enhancement factors (with respect to the reference sample) in the 22−190 range were obtained, indicating that light absorption is strongly enhanced in present core−shell nanowires, and further depending on the actual value of AlGaAs shell thickness. Comparison with results of FDTD studies on GaAs nanowire arrays and single GaAs−AlGaAs core−shell nanowires in the literature allowed us to ascribe our findings to improved wave-guiding of incident light ($\lambda \sim 876$ nm) into the GaAs cores induced by the surrounding AlGaAs shells. Present results further point out that light concentration into GaAs nanowires could be greatly increased by careful engineering of the shell bandgap energy (e.g., its refractive index), thickness, and array density. In conclusion, we confirm the great potential of dense arrays of core−shell nanowires as superabsorptive media for the fabrication of efficient and less costly III-V solar cells.

ASSOCIATED CONTENT

Supporting Information

The Supporting Information is available free of charge at https://pubs.acs.org/doi/10.1021/acsanm.2c04044.

Crystal phase determination and extended defects of GaAs−AlGaAs core−shell nanowires; strain-induced energy splitting of the GaAs core LH- and HH-exciton resonances; estimation of inhomogeneous broadening of the HH- and LH-exciton resonances; and estimation of the GaAs core volume fill fraction in dense core−shell nanowire arrays (PDF)

AUTHOR INFORMATION

Corresponding Author

Nico Lovergine − *Dipartimento di Ingegneria dell'Innovazione, Università del Salento, I-73100 Lecce, Italy*; orcid.org/0000-0003-0190-4899; Phone: +390 832 297234; Email: nicola.lovergine@unisalento.it; Fax: +390 832 297249

Authors

Arianna Cretì − *Institute for Microelectronics and Microsystems, National Research Council (IMM-CNR), I-73100 Lecce, Italy*; orcid.org/0000-0003-0389-660X

https://doi.org/10.1021/acsanm.2c04044
ACS Appl. Nano Mater. 2022, 5, 18149−18158

Paola Prete − *Institute for Microelectronics and Microsystems, National Research Council (IMM-CNR), I-73100 Lecce, Italy;* orcid.org/0000-0002-4948-4718

Mauro Lomascolo − *Institute for Microelectronics and Microsystems, National Research Council (IMM-CNR), I-73100 Lecce, Italy;* orcid.org/0000-0002-2851-8552

Complete contact information is available at: https://pubs.acs.org/10.1021/acsanm.2c04044

Author Contributions

[§]A.C. and P.P. equally contributed.

Funding

This work was supported by the Regional Government of Puglia within the framework of the Public Research Laboratory Network "III Generation Photovoltaics based on Nanostructured Semiconductors and Hybrid Nanocomposites Materials (PHASHYN)", Project No. 35.

Notes

The authors declare no competing financial interest.

■ ACKNOWLEDGMENTS

The authors would like to thank F. Marzo for FE-SEM observations and G. Montagna for his great technical help.

■ REFERENCES

(1) Mayer, B.; Rudolph, D.; Schnell, J.; Morkötter, S.; Winnerl, J.; Treu, J.; Müller, K.; Bracher, G.; Abstreiter, G.; Koblmüller, G.; Finley, J. J. Lasing from individual GaAs-AlGaAs core-shell nanowires up to room temperature. *Nat. Commun.* **2013**, *4*, 2931.

(2) Gallo, E. M.; Chen, G.; Currie, M.; McGuckin, T.; Prete, P.; Lovergine, N.; Nabet, B.; Spanier, J. E. Picosecond response times in GaAs/AlGaAs core/shell nanowire-based photodetectors. *Appl. Phys. Lett.* **2011**, *98*, 241113.

(3) Persano, A.; Nabet, B.; Taurino, A.; Prete, P.; Lovergine, N.; Cola, A. Polarization anisotropy of individual core/shell GaAs/AlGaAs nanowires by photocurrent spectroscopy. *Appl. Phys. Lett.* **2011**, *98*, 153106.

(4) Czaban, J. A.; Thompson, D. A.; LaPierre, R. R. GaAs core-shell nanowires for photovoltaic applications. *Nano Lett.* **2009**, *9*, 148−154.

(5) Mariani, G.; Scofield, A. C.; Hung, C.-H.; Huffaker, D. L. GaAs nanopillar-array solar cells employing in situ surface passivation. *Nat. Commun.* **2013**, *4*, 1497.

(6) Åberg, I.; Vescovi, G.; Asoli, D.; Naseem, U.; Gilboy, J. P.; Sundvall, C.; Dahlgren, A.; Svensson, K. E.; Anttu, N.; Björk, M. T.; Samuelson, L. A GaAs nanowire array solar cell with 15.3% efficiency at 1 sun. *IEEE J. Photovoltaics* **2016**, *6*, 185−190.

(7) van Dam, D.; van Hoof, N. J. J.; Cui, Y.; van Veldhoven, P. J.; Bakkers, E. P. A. M.; Gomez Rivas, J.; Haverkort, J. E. M. High-efficiency nanowire solar cells with omnidirectionally enhanced absorption due to self-aligned indium−tin−oxide Mie scatterers. *ACS Nano* **2016**, *10*, 11414−11419.

(8) Brongersma, M. L.; Cui, Y.; Fan, S. Light management for photovoltaics using high index nanostructures. *Nat. Mater.* **2014**, *13*, 451−460.

(9) Wen, L.; Zhao, Z.; Li, X.; Shen, Y.; Guo, H.; Wang, Y. Theoretical analysis and modeling of light trapping in high efficiency GaAs nanowire array solar cells. *Appl. Phys. Lett.* **2011**, *99*, 143116.

(10) Bao, H.; Ruan, X. Optical absorption enhancement in disordered vertical silicon nanowire arrays for photovoltaic applications. *Opt. Lett.* **2010**, *35*, 3378−3380.

(11) Gu, Z.; Prete, P.; Lovergine, N.; Nabet, B. On optical properties of GaAs/AlGaAs core-shell periodic nanowire arrays. *J. Appl. Phys.* **2011**, *109*, No. 064314.

(12) Krogstrup, P.; Jørgensen, H.; Heiss, M.; Demichel, O.; Holm, J. V.; Aagesen, M.; Nygard, J.; Fontcuberta i Morral, A. Single-nanowire solar cells beyond the Shockley−Queisser limit. *Nat. Photonics* **2013**, *7*, 306−310.

(13) Wang, S.; Yan, X.; Zhang, X.; Li, J.; Ren, X. Axially connected nanowire core-shell p-n junctions: a composite structure for high-efficiency solar cells. *Nanoscale Res. Lett.* **2015**, *10*, 22.

(14) Prete, P.; Lovergine, N. Dilute nitride III-V nanowires for high-efficiency intermediate-band photovoltaic cells: Materials requirements, self-assembly methods and properties. *Prog. Cryst. Growth Charact. Mater.* **2020**, *66*, No. 100510.

(15) Di Carlo, V.; Prete, P.; Dubrovskii, V.B.; Berdnikov, Y.; Lovergine, N. CdTe nanowires by Au-catalyzed metalorganic vapor phase epitaxy. *Nano Lett.* **2017**, *17*, 4075−4082.

(16) Mann, S. A.; Sciacca, B.; Zhang, Y.; Wang, J.; Kontoleta, E.; Liu, H.; Garnett, E. C. Integrating sphere microscopy for direct absorption measurements of single nanostructures. *ACS Nano* **2017**, *11*, 1412−1418.

(17) Diedenhofen, S. L.; Janssen, O. T. A.; Grzela, G.; Bakkers, E. P. A. M.; Rivas, J. G. Strong geometrical dependence of the absorption of light in arrays of semiconductor nanowires. *ACS Nano* **2011**, *5*, 2316−2323.

(18) Scuderi, M.; Prete, P.; Lovergine, N.; Spinella, C.; Nicotra, G. Effects of VLS and VS mechanisms during shell growth in GaAs-AlGaAs core-shell nanowires investigated by transmission electron microscopy. *Mater. Sci. Semicond. Process.* **2017**, *65*, 108−112.

(19) Prete, P.; Marzo, F.; Paiano, P.; Lovergine, N.; Salviati, G.; Lazzarini, L.; Sekiguchi, T. Luminescence of GaAs/AlGaAs core-shell nanowires grown by MOVPE using tertiarybutylarsine. *J. Cryst. Growth* **2008**, *310*, 5114−5118.

(20) Paiano, P.; Prete, P.; Speiser, E.; Lovergine, N.; Richter, W.; Tapfer, L.; Mancini, A. M. GaAs nanowires grown by Au-catalyst-assisted MOVPE using tertiarybutylarsine as group-V precursor. *J. Cryst. Growth* **2007**, *298*, 620−624.

(21) Paiano, P.; Prete, P.; Lovergine, N.; Mancini, A. M. Size and shape control of GaAs nanowires grown by metalorganic vapor phase epitaxy using tertiarybutylarsine. *J. Appl. Phys.* **2006**, *100*, No. 094305.

(22) Wolf, D.; Hübner, R.; Niermann, T.; Sturm, S.; Prete, P.; Lovergine, N.; Büchner, B.; Lubk, A. Three-dimensional composition and electric potential mapping of III-V core-multishell nanowires by correlative STEM and holographic tomography. *Nano Lett.* **2018**, *18*, 4777−4784.

(23) Lubk, A.; Wolf, D.; Prete, P.; Lovergine, N.; Niermann, T.; Sturm, S.; Lichte, H. Nanometer-scale tomographic reconstruction of three-dimensional electrostatic potentials in GaAs/AlGaAs core-shell nanowires. *Phys. Rev. B* **2014**, *90*, No. 125404.

(24) Pavesi, L.; Guzzi, M. Photoluminescence of $Al_xGa_{1-x}As$ alloys. *J. Appl. Phys.* **1994**, *75*, 4779−4842.

(25) The optical absorption coefficient of the $Al_{0.33}Ga_{0.67}As$ alloy at the 632.8 nm (1.959 eV) line is reported to range between 1.7×10^4 cm^{-1} [Monemar, B.; Shih, K. K.; Pettit, G. D. *J. Appl. Phys.*1976, *47*, 2604−2613] and 2.6×10^4 cm^{-1} [Aspnes, D. E.; Kelso, S. M.; Logan, R. A.; Bath, R. *J. Appl. Phys.*1986, *60*, 754−767]. Considering a value of absorption of 2.6×10^4 cm^{-1} the optical transmissivity for a 215-nm thick AlGaAs layer is ∼60%. This ensures that the laser modulation beam is not completely absorbed by the AlGaAs layer and that the PR signal originating in the GaAs should be visible.

(26) Tyan, S. L.; Wang, Y. C.; Hwang, J. S.; Shen, H. Unambiguous photoreflectance determination of electric fields using phase suppression. *Appl. Phys. Lett.* **1996**, *68*, 3452−3454.

(27) Wang, Y. C.; Chou, W. Y.; Hwang, W. C.; Hwang, J. S. Electric fields separation by phase selection in modulation spectroscopy of photoreflectance. *Solid State Commun.* **1997**, *104*, 717−721.

(28) Ganzha, A. V.; Kus'menko, R. V.; Kircher, K.; Schreiber, J.; Hildebrandt, S. Lock-in-phase analysis of n-GaAs photoreflectance spectra. *Semiconductors* **1998**, *32*, 245−249.

(29) Kudrawiec, R.; Misiewicz, J.Optical Modulation Spectroscopy, Chapter 4, p. 95, In Patanè, A.; Balkan, N., Eds., *Semiconductor Research*, Springer Series in Materials Science 150, Springer-Verlag Berlin Heidelberg, 2012.

(30) Misiewicz, J.; Sitarek, P.; Sek, G. Photoreflectance spectroscopy of low-dimensional semiconductor structures. *Opto-Electron. Rev.* **2000**, *8*, 1−24.
(31) Shen, H.; Dutta, M. Franz-Keldysh oscillations in modulation spectroscopy. *J. Appl. Phys.* **1995**, *78*, 2151−2176.
(32) Shanabrook, B. V.; Glembocki, O. J.; Beard, W. T. Photoreflectance modulation mechanisms in GaAs/AlGaAs multiple quantum wells. *Phys. Rev. B* **1987**, *35*, 2540−2543.
(33) Shen, H.; Pan, S. H.; Pollak, F. H.; Dutta, M.; Au Coin, T. R. Conclusive evidence for miniband dispersion in the photoreflectance of a GaAs/GaAlAs coupled multiple-quantum-well structure. *Phys. Rev. B* **1987**, *36*, 9384−9387.
(34) Theis, M.; Sanders, G. D.; Leak, C. E.; Bajaj, K. K.; Morkoç, H. Excitonic transitions in GaAs/GaAlAs quantum wells observed by photoreflectance spectroscopy: Comparison with a first-principles theory. *Phys. Rev. B* **1988**, *37*, 3042−3051.
(35) Huang, Y. S.; Qiang, H.; Pollak, F. H.; Lee, J.; Elman, B. Electroreflectance study of a symmetrically coupled GaAs/GaAlAs double quantum well system. *J. Appl. Phys.* **1991**, *70*, 3808−3814.
(36) Temme, N. M. The numerical computation of the Confluent Hypergeometric Function U(a,b,z). *Numer. Math.* **1983**, *41*, 63.
(37) Aspnes, D. E.*Handbook on Semiconductors*, Balkanski, M., Ed., North-Holland, Amsterdam, 1980, Vol 2; p 109.
(38) Hosea, T. J. C. *Phys. Status Solidi B* **1994**, *182*, K43.
(39) Miccoli, I.; Prete, P.; Marzo, F.; Cannoletta, D.; Lovergine, N. Synthesis of vertically-aligned GaAs nanowires on GaAs/(111)Si hetero-substrates by metalorganic vapour phase epitaxy. *Cryst. Res. Technol.* **2011**, *46*, 795−800.
(40) Chang, B.; Zhao, D. Direct assembly of nanowires by electron beam-induced dielectrophoresis. *Nanotechnology* **2021**, *32*, 415602.
(41) Miccoli, I.; Prete, P.; Lovergine, N. Mass-transport driven growth dynamics of AlGaAs shells deposited around dense GaAs nanowires by metalorganic vapor phase epitaxy. *CrystEngComm* **2015**, *17*, 5998−6005.
(42) Prete, P.; Wolf, D.; Marzo, F.; Lovergine, N. Nano-scale spectroscopic imaging of GaAs-AlGaAs quantum well tube nanowires: correlating luminescence with nanowire size and inner multi-shell structure. *Nanophotonics* **2019**, *8*, 1567−1577.
(43) Theis, M.; Sanders, G. D.; Evans, K. R.; Liou, L. L.; Leak, C. E.; Bajaj, K. K.; Stutz, C. E.; Jones, R. L.; Chang, Y.-C. Extrinsic contributions to photoreflectance of AlGaAs/GaAs quantum wells: An investigation of the "donor-related" feature. *Phys. Rev. B* **1989**, *39*, 11038−11043.
(44) Brierley, S. K.; Lehr, D. S. Correlation between the photoreflectance impurity peak in semi-insulating GaAs and bulk acceptor concentration. *J. Appl. Phys.* **1990**, *67*, 3878−3880.
(45) Yin, X.; Pollak, F. H.; Pawlowicz, L.; O'Neill, T.; Hafizi, M. Characterization of GaAs/GaAlAs heterojunction bipolar transistor structures using photoreflectance. *Appl. Phys. Lett.* **1990**, *56*, 1278−1280.
(46) Arab, S.; Yao, M.; Zhou, C.; Dapkus, P. D.; Cronin, S. B. Doping concentration dependence of photoluminescence spectra of n-type GaAs nanowires. *Appl. Phys. Lett.* **2016**, *108*, 182106.
(47) Vurgaftman, I.; Meyer, J. R.; Ram-Mohan, L. R. J. Band parameters for III−V compound semiconductors and their alloys. *J. Appl. Phys.* **2001**, *89*, 5815−5875.
(48) *Semiconductors-Basic Data*; Madelung, O., Ed., Spinger-Verlag Berlin Heidelberg New York, 1996, ISBN 3-540-60883-4.
(49) Huang, D.; Mui, D.; Morkoc, H. Interference effects probed by photoreflectance spectroscopy. *J. Appl. Phys.* **1989**, *66*, 358−361.
(50) Kallergi, N.; Roughani, J.; Aubel, J.; Sundaram, S. Correlation of interference effects in photoreflectance spectra with GaAs homolayer thickness. *J. Appl. Phys.* **1990**, *68*, 4656−4661.
(51) Lipsanen, H. K.; Airaksinen, V. M. Interference effects in photoreflectance of epitaxial layers grown on semi-insulating substrates. *Appl. Phys. Lett.* **1993**, *63*, 2863−2865.
(52) Chen, G.; Gallo, E. M.; Burger, J.; Nabet, B.; Cola, A.; Prete, P.; Lovergine, N.; Spanier, J. E. On direct-writing methods for electrically contacting GaAs and Ge nanowire devices. *Appl. Phys. Lett.* **2010**, *96*, 223107.
(53) Sing, J.*Electronic and Optoelectronic properties of Semiconductors Structures*, Cambridge University Press, 2012, ISBN 0 521 82379 X.
(54) Bastard, G.*Wave mechanics applied to semiconductor heterostructures*, Les Éditions de Physique, 1988. ISBN 0470217081.
(55) Casey, H. C., Jr.; Sell, D. D.; Wecht, K. W. Concentration dependence of the absorption coefficient for n− and p−type GaAs between 1.3 and 1.6 eV. *J. Appl. Phys.* **1975**, *46*, 250−257.
(56) Hocevar, M.; Giang, L. T. T.; Songmuang, R.; den Hertog, M.; Besombes, L.; Bleuse, J.; Niquet, Y.-M.; Pelekanos, N. T. Residual strain and piezoelectric effects in passivated GaAs/AlGaAs coreshell nanowires. *Appl. Phys. Lett.* **2013**, *102*, 191103.
(57) Prete, P.; Miccoli, I.; Marzo, F.; Lovergine, N. Built-in elastic strain and localization effects on GaAs luminescence of MOVPE-grown GaAs−AlGaAs core−shell nanowires. *Phys. Status Solidi RRL* **2013**, *7*, 874−877.
(58) Aspnes, D. E.; Kelso, S. M.; Logan, R. A.; Bath, R. Optical properties of $Al_xGa_{1-x}As$. *J. Appl. Phys.* **1986**, *60*, 754−767.